steel research international

Toward Modeling of Electrochemical Reactions during Electroslag Remelting (ESR) Process

Ebrahim Karimi-Sibaki, Abdellah Kharicha, Menghuai Wu,* Andreas Ludwig, and Jan Bohacek

Electrochemical reactions always occur at the electrode–slag and slag–metal melt interfaces during the electroslag remelting (ESR) process. However, those reactions together with the ion transport phenomenon in the molten slag region are still poorly understood. A numerical model considering both the ion transport and the electrochemical reactions is demanding. For this purpose, a numerical model is proposed. The ion transport is modeled by solving the Poisson–Nernst–Planck (PNP) equations, while the kinetics of the reaction at the slag–metal interface is modeled with the well-known "Butler–Volmer" formula. Demonstratively, a one- dimensional case is calculated: a DC electric current is applied to a molten multi-ion slag (CaF_2–FeO) between the anode and the cathode. The modeling results show that the redox reaction occurs only for the ferrous ion (Fe^{2+}), not for other ions at low current density ($<2\,kA\,m^{-2}$), which was verified experimentally. We also find that formation of ferric iron (Fe^{3+}) or discharge of calcium at large current density ($>5\,kA\,m^{-2}$) may not take place, although some researchers have proposed such a hypothesis. Therefore, further research steps are suggested to verify this point so that the model is fully applicable for the industrial ESR process.

1. Introduction

The Electroslag Remelting (ESR) process is a secondary metallurgical process for manufacturing superior quality alloys such as Nickel base, Titanium base, and stainless steel. A shown in **Figure 1**, the process is used to refine a consumable metal electrode through a molten slag that is electrically heated. The thermal energy (Joule heating) is provided to the process that leads to remelting of the electrode and formation of droplets. Then, droplets pass through the slag and enter to the melt pool. Eventually, the melt pool solidifies in a water-cooled mold to produce the high-grade ingot.

Over the past decades, different numerical models have been proposed to describe flow, thermal, magnetic fields, as well as solidification of ingots during the electroslag remelting (ESR) process.[1–5] Modeling attempts were made for the chemical and electrochemical reactions in the slag by means of thermodynamics and a kinetic modeling approach.[6–7] Calcium fluoride-based slags, typically composed of CaF_2, CaO, Al_2O_3, SiO_2, MgO, and FeO, are mostly used to protect the liquid metal against the surrounding air; to provide heat through Joule heating into the process, and to remove impurities such as sulphur and non-metallic inclusions from the alloy. High chemical reactivity and electrical resistivity (low electrical conductivity) are favorable properties of the slag. Evidently, the ion transport plays an important role in the electrical conductivity of the slag.[8–9] Additionally, several electrochemical reactions such as a calcium discharge at the melt pool–slag interface or formation of ferric iron (Fe^{3+}) at electrode–slag interface (Figure 1) may take place. Mitchell et al.[10] evaluated the electrochemical concentration overpotential at the interface among an iron electrode and CaF_2-based slags such as CaF_2–CaO, CaF_2–Al_2O_3, etc. They found some correlations between the ionic properties of the slag, the distribution of oxygen in the ingot, and loss of alloying elements during the DC operation of the ESR process.[11] The melting behavior of an ESR electrode is notably influenced by electrochemical reactions.[12–14] For instance, the melt rate of a cathodic (negative) electrode was reported to be lower than that of the anodic (positive) electrode during the ESR process as run under DC current.[15] Apparently, electrochemical reactions at the slag–metal interface and transport of ions within the slag are crucial.

In this paper, we employed a Finite Volume Method (FVM)-based numerical model to solve the governing

[*] M. Wu, E. Karimi-Sibaki, A. Kharicha
Christian-Doppler Lab for Advanced Process Simulation of Solidification and Melting, Montanuniversitaet of Leoben, Franz-Josef-Str. 18, A-8700 Leoben, Austria
Email: menghuai.wu@unileoben.ac.at
A. Kharicha, M. Wu, A. Ludwig, J. Bohacek
Chair of Simulation and Modeling of Metallurgical Processes, Montanuniversitaet of Leoben, Franz-Josef-Str. 18, A-8700 Leoben, Austria

DOI: 10.1002/srin.201700011

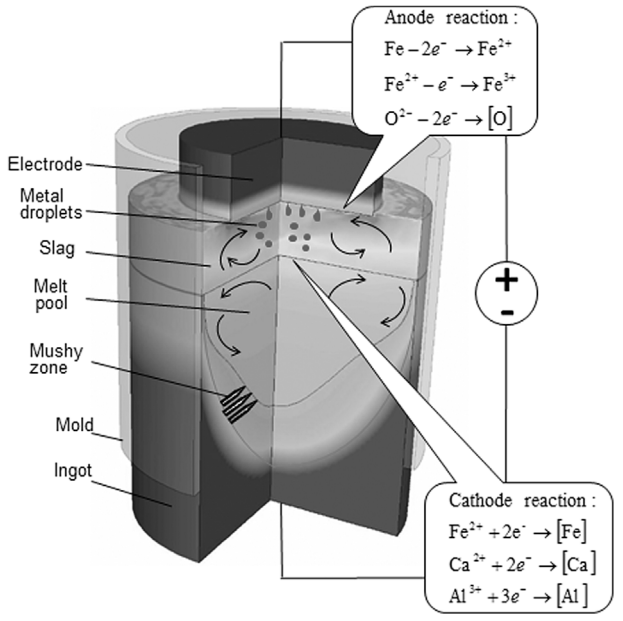

Figure 1. Schematic representation of electroslag remelting (ESR) process and involving feasible electrochemical reactions at slag–electrode and slag–melt pool interfaces.

Poisson–Nernst–Planck (PNP) equations which describe the electrochemical transport of ions in the bulk of the slag (electrolyte). The well-known "Butler–Volmer" equation is implemented to model the electrochemical reactions which occur at electrode–slag interface. Our proposed numerical model can be efficiently used to investigate complex electrochemical systems involving multiple ions. The model enables us to directly calculate vital parameters of the system such as the Ohmic potential drop, activation, and concentration overpotentials. Additionally, the key field structures including concentrations of ions, electric potential, and charge density fields across the electrolyte can be computed. Eventually, the obtained modeling results helps to propose a possible explanation for the relation between the polarity (positive or negative) and melt rate of the electrode in the DC ESR process.

2. Mathematical Model

2.1. General Equations

The electrochemical transport of ions in the bulk of the electrolyte which is subjected to an electric field is described according to the Poisson–Nernst–Planck (PNP) equations:

$$-\nabla \cdot (\varepsilon_s \nabla \phi) = F \sum z_i c_i \tag{1}$$

$$\frac{\partial c_i}{\partial t} = -\nabla \cdot \vec{N}_i \tag{2}$$

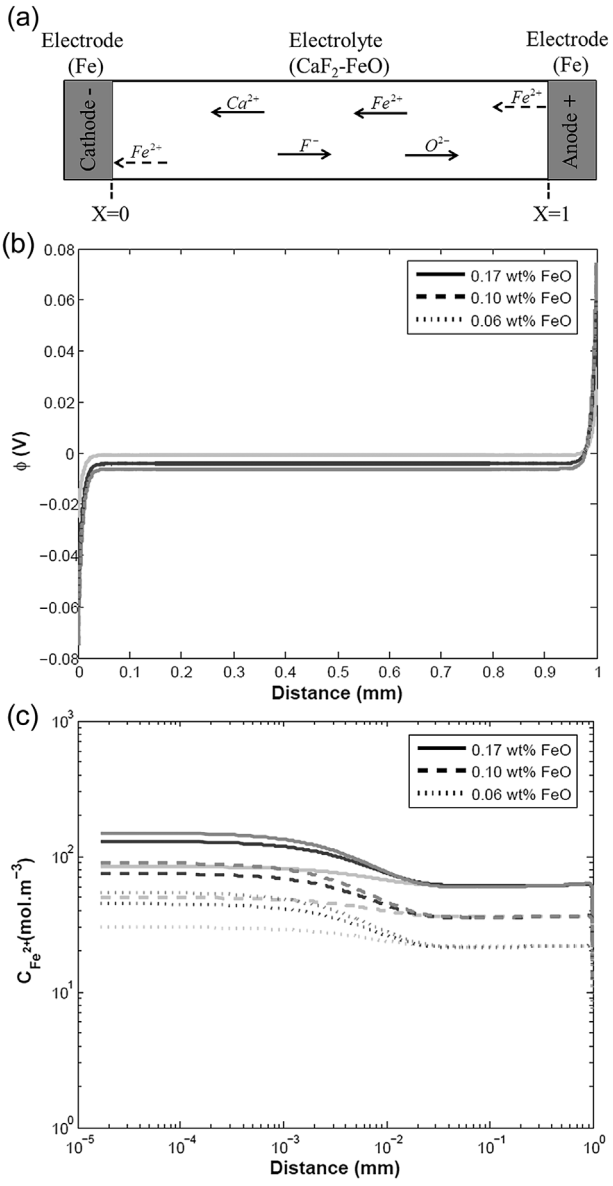

Figure 2. a) Schematic representation of the CaF_2–FeO electrochemical system in which the slag is fully dissociated and only ferrous ion (Fe^{2+}) participates in Faradaic reaction; cathode is located at $x = 0$, and anode is located at $x = 1$. Following parameters are plotted across the electrolyte (CaF_2–FeO) considering different bulk concentration of FeO (0.06, 0.10, and 0.17 wt% FeO) and various applied voltages including: 0.07 (gray), 0.12 (black), and 0.15 V (dark gray): b) electric potential, c) concentration of ferrous ion.

$$\vec{N}_i = \vec{u}c_i - D_i \nabla c_i - \frac{F z_i D_i \nabla \phi}{RT} c_i \tag{3}$$

The relationship between the electric potential (ϕ) and charge density ($\rho = F \sum z_i c_i$) is given by the Poisson equation, Equation 1, where ε_s is the electric permittivity of the electrolyte. The charge density is calculated using the Faraday constant (F) as well as concentration (c_i) and

1. Governing equations:

$$\frac{\partial}{\partial x}\left(-\zeta^2\frac{\partial\phi^*}{\partial x}\right)=z_{Ca^{2+}}C_{Ca^{2+}}+z_{Fe^{2+}}C_{Fe^{2+}}+z_{F^-}C_{F^-}+z_{O^{2-}}C_{O^{2-}},$$

$$\frac{\partial C_{Ca^{2+}}}{\partial t}=\frac{\partial}{\partial x}\left(D_{Ca^{2+}}\frac{\partial C_{Ca^{2+}}}{\partial x}+z_{Ca^{2+}}D_{Ca^{2+}}C_{Ca^{2+}}\frac{\partial\phi^*}{\partial x}\right),$$

$$\frac{\partial C_{Fe^{2+}}}{\partial t}=\frac{\partial}{\partial x}\left(D_{Fe^{2+}}\frac{\partial C_{Fe^{2+}}}{\partial x}+z_{Fe^{2+}}D_{Fe^{2+}}C_{Fe^{2+}}\frac{\partial\phi^*}{\partial x}\right),$$

$$\frac{\partial C_{O^{2-}}}{\partial t}=\frac{\partial}{\partial x}\left(D_{O^{2-}}\frac{\partial C_{O^{2-}}}{\partial x}+z_{O^{2-}}D_{O^{2-}}C_{O^{2-}}\frac{\partial\phi^*}{\partial x}\right),$$

$$\frac{\partial C_{F^-}}{\partial t}=\frac{\partial}{\partial x}\left(D_{F^-}\frac{\partial C_{F^-}}{\partial x}+z_{F^-}D_{F^-}C_{F^-}\frac{\partial\phi^*}{\partial x}\right),$$

$$\zeta=\frac{\lambda_D}{L_{ref}},\ \lambda_D=\sqrt{\frac{\varepsilon_s RT}{2z^2F^2C_{ref}}},\ \phi^*=\frac{F\phi}{RT},$$

$$C_i=\frac{c_i}{C_{ref}},\ i=Ca^{2+},\ F^-,\ Fe^{2+},\ or\ O^{2-}$$

2. Boundary conditions:

$$\phi^*(0)=-\frac{F}{2RT}\left[V_{app}(0)+\lambda_s\frac{\partial\phi}{\partial x}(0)\right],$$

$$\phi^*(1)=+\frac{F}{2RT}\left[V_{app}(1)-\lambda_s\frac{\partial\phi}{\partial x}(1)\right],$$

$$D_{Ca^{2+}}\frac{\partial C_{Ca^{2+}}}{\partial x}(0,1)+z_{Ca^{2+}}D_{Ca^{2+}}C_{Ca^{2+}}(0,1)\frac{\partial\phi^*}{\partial x}(0,1)=0,$$

$$D_{F^-}\frac{\partial C_{F^-}}{\partial x}(0,1)+z_{F^-}D_{F^-}C_{F^-}(0,1)\frac{\partial\phi^*}{\partial x}(0,1)=0,$$

$$D_{O^{2-}}\frac{\partial C_{O^{2-}}}{\partial x}(0,1)+z_{O^{2-}}D_{O^{2-}}C_{O^{2-}}(0,1)\frac{\partial\phi^*}{\partial x}(0,1)=0,$$

$$D_{Fe^{2+}}\frac{\partial C_{Fe^{2+}}}{\partial x}(0,1)+z_{Fe^{2+}}D_{Fe^{2+}}C_{Fe^{2+}}(0,1)\frac{\partial\phi^*}{\partial x}(0,1)=\pm\frac{j}{z_{Fe^{2+}}C_{ref}F},$$

3. System parameters

$$j=j_0\left[\exp\left(\frac{(1-\alpha)nF\eta_s}{RT}\right)-\exp\left(-\frac{\alpha nF\eta_s}{RT}\right)\right],\ \eta_s=-\lambda_s\frac{\partial\phi}{\partial x},$$

$$\eta_{AR}=\frac{RT}{nF}\ln\left(\frac{c^A_{Fe^{2+}}}{\bar{c}_{Fe^{2+}}}\right),\ \eta_{RC}=\frac{RT}{nF}\ln\left(\frac{\bar{c}_{Fe^{2+}}}{c^C_{Fe^{2+}}}\right),$$

$$\eta_{AC}=\eta_{AR}+\eta_{RC}=\frac{RT}{nF}\ln\left(\frac{c^A_{Fe^{2+}}}{c^C_{Fe^{2+}}}\right),\ iR=V_{app}-\eta_{AC},$$

$$\beta=\frac{\exp\left(\frac{nF\eta_{AC}}{RT}\right)-1}{\exp\left(\frac{nF\eta_{AC}}{RT}\right)+1}.$$

Symbols:
Calcium ion (Ca^{2+}),
Fluoride ion (F^-),
Ferrous ion (Fe^{2+}),
Oxygen ion (O^{2-}),
Time (t), distance (x),
Debye screening length (λ_D),
Reference length (L_{ref}),
Reference concentration (C_{ref}),
Electric permittivity (ε_s),
Universal gas constant (R),
Temperature (T),
Charge number of each ion (z),
Faraday constant (z)
Electric potential (ϕ),
Dimensionless electric potential (ϕ^*),
Concentration of each ion (c_i),
Dimensionless concentration of each ion (C_i),
Diffusion coefficient of each ion (D),
Applied voltage (V_{app}),
Effective stern width (λ_s),
Current density (j),
Exchange current density (j_0),
Charge transfer coefficient (α),
Number of exchanged electrons (n),
Activation overpotential (η_s),
Anodic concentration overpotential (η_{AR}),
Cathodic concentration overpotential (η_{RC}),
Total concentration overpotential (η_{AC}),
Concentration of ferrous ion at anode ($c^A_{Fe^{2+}}$),
Concentration of ferrous ion at cathode ($c^C_{Fe^{2+}}$),
Concentration of ferrous ion in the bulk of slag ($\bar{c}_{Fe^{2+}}$),
Ohmic voltage drop (iR)

Table 1. Governing Poisson–Nernst–Planck (PNP) equations, related boundary conditions, and pertaining parameters for CaF_2–FeO electrochemical system.

charge number (z_i) of i-th ion. According to the conservation equation, Equation 2, the total flux of i-th ion (N_i) including convection, diffusion, and electro-migration must be conserved. The convection and diffusion fluxes are dependent on the velocity ($\vec{u}$) and diffusion coefficient (D_i). The electro-migration flux takes into account the transport of electroactive (non-zero charge number) ions as described in Equation 3 where R and T denote universal gas constant and temperature, respectively.

Note that the formulation of the problem is not complete before assigning the appropriate boundary conditions to the PNP equations. Assuming a stagnant electrolyte ($u=0$), the total flux of diffusion and electro-migration at boundaries for non-reacting ions is assigned to zero. However, the boundary flux of the reacting ion is related to the current density that in turn is dependent on the activation overpotential (η) and exchange current density (j_0) through the "Butler–Volmer" equation,[16]

$$N_R=\pm\frac{nj}{z_RF} \tag{4}$$

$$j = j_0\left[\exp\left(\frac{(1-\alpha)nF\eta}{RT}\right) - \exp\left(-\frac{\alpha nF\eta}{RT}\right)\right] \quad (5)$$

where N_R and z_R are the total flux and charge number of the reacting ion which is produced (+) or consumed (–) at the electrode–electrolyte interface. Furthermore, n and α denote number of exchanged electrons and charge transfer coefficient, respectively.

The boundary conditions for the Poisson equation are considered according to the potentiostatic technique, in which the applied voltage is given and the current density is computed in a self-consistent manner.[16] The electric double layer (EDL), which appears on the surface of electrode, is subjected to an electric field consists of a stern layer, a diffusion layer, and a diffuse charge layer. The potential drop across the compact stern layer determines the activation overpotential, whereas the concentration of the reactive ion at the surface of electrode governs the amount of concentration overpotential.[17,18]

2.2. CaF_2–FeO System

In the current study, the capability of our model to capture the aforementioned parameters such as activation and concentration overpotentials for an electrochemical system is demonstrated. As an example, we calculate the system of CaF_2–FeO slag operating under a DC voltage, which involves non-reacting ions of Ca^{+2}, O^{2-}, F^- and the reacting ferrous ion (Fe^{2+}). The system consists of the slag (electrolyte) that is confined by two parallel and planar iron electrodes as shown schematically in **Figure 2**a. The slag is assumed to be fully dissociated and stagnant ($u = 0$). Furthermore, the ferrous ion participates in Faradaic reactions at the electrode–slag interface,

$$CaF_2 \rightarrow Ca^{2+} + 2F^- \quad (6)$$

$$FeO \rightarrow Fe^{2+} + O^{2-} \quad (7)$$

$$(\text{At anode}): Fe \rightarrow Fe^{2+} + 2e^- \quad (8)$$

$$(\text{At cathode}): Fe^{2+} + 2e^- \rightarrow Fe \quad (9)$$

The cathode is located at $x = 0$, and the anode is located at $x = 1$. It is appropriate to formulate the PNP equations regarding our electrochemical system in a one-dimensional model. All governing equations, boundary conditions, and relevant parameters are summarized in **Table 1**. The size of the computational domain is 1 mm, which includes 1000 grid nodes. Details of the mathematical model were described in ref.[19,20]

The transport of each ion due to diffusion and electromigration is described by a conservation equation (Nernst–Planck). In addition, the electric potential is coupled to concentrations of ions through Poisson equation. Therefore, a total number of five coupled and nonlinear equations are simultaneously solved. All parameters such as diffusion coefficient, charge number, effective stern length used in our calculations are summarized in **Table 2**.

Parameter	
$R(J \cdot K^{-1} \cdot mol^{-1})$	8.314546
$T(K)$	1723[22]
$F(A \cdot s \cdot mol^{-1})$	96 485
$V_{app}(V)$	Variable (**Table 3**)
$\varepsilon_s(F \cdot m^{-1})$	8.85418×10^{-12}
$C_{ref}(mol \cdot m^{-3})$	10^5
$L_{ref}(m)$	10^{-3}
$\lambda_D(m)$	10^{-9}[17]
$\lambda_s(m)$	10^{-8}[20]
α	0.6[22]
ζ	10^{-5}[20]
n	2
$j_0(kA \cdot m^{-2})$	Variable (Table 3)
$\bar{c}_{Ca^{2+}}(mol \cdot m^{-3})$	0.333×10^5
$D_{Ca^{2+}}(m^2 \cdot s^{-1})$	5.66×10^{-9}[23]
$z_{Ca^{2+}}$	+2
$\bar{c}_{F^-}(mol \cdot m^{-3})$	0.666×10^5
$D_{F^-}(m^2 \cdot s^{-1})$	4.12×10^{-9}[23]
z_{F^-}	–1
$\bar{c}_{Fe^{2+}}(mol \cdot m^{-3})$	Variable (Table 3)
$D_{Fe^{2+}}(m^2 \cdot s^{-1})$	2.3×10^{-9}[21]
$z_{Fe^{2+}}$	+2
$\bar{c}_{O^{2-}}(mol \cdot m^{-3})$	$\bar{c}_{Fe^{2+}}(mol \cdot m^{-3})$
$D_{O^{2-}}(m^2 \cdot s^{-1})$	2.5×10^{-9}[23]
$z_{O^{2-}}$	–2

Table 2. System properties and operational parameters used in our calculations.

3. Results and Discussions

We performed an extensive series of simulations to investigate the relationship between concentration of the reacting ion in

Input					Output						
$Wt.\%FeO$	$\bar{c}_{Fe^{2+}}(mol \cdot m^{-3})$	$j_0(kA \cdot m^{-2})$	$V_{app}(V)$	$\eta_s(mV)$	$j(A \cdot m^{-2})$	$c^A_{Fe^{2+}}(mol \cdot m^{-3})$	$c^C_{Fe^{2+}}(mol \cdot m^{-3})$	$\eta_{AR}(V)$	$\eta_{RC}(V)$	$\eta_{AC}(V)$	$iR(V)$
0.024	8.96[21]	40[21]	0.5	0.36	193	0.16	123.4	0.298	0.194	0.492	0.008
			0.7	0.59	317	0.028	293.2	0.427	0.258	0.685	0.015
			1	1.14	616	0.003	998.6	0.592	0.348	0.941	0.059
			1.1	1.4	758	0.00196	1463.2	0.624	0.377	1.0	0.1
			1.2	1.71	925.5	0.00155	2077.4	0.641	0.403	1.044	0.156
			1.3	2.1	1121	0.0014	2951.3	0.649	0.429	1.078	0.222
			1.4	2.49	1347	0.00133	4030.4	0.652	0.452	1.104	0.296
			1.5	2.95	1594	0.0013	5433.4	0.654	0.474	1.128	0.372
0.06[22]	21.7	80[24]	0.05	0.03	32.7	15.4	29.9	0.025	0.0237	0.049	0.001
			0.07	0.042	45.8	13.4	33.7	0.035	0.0326	0.068	0.002
			0.12	0.073	78.7	9.4	44.8	0.062	0.0536	0.116	0.004
			0.15	0.092	99.2	7.3	54.2	0.081	0.068	0.147	0.003
			0.2	0.124	133.3	5.0	69.4	0.11	0.086	0.194	0.006
0.1[22]	36.1	280[24]	0.05	0.03	114.4	25.6	49.7	0.025	0.0236	0.049	0.001
			0.07	0.042	160.2	22.3	55.9	0.036	0.0324	0.069	0.001
			0.12	0.073	276.1	15.4	74.7	0.063	0.0538	0.116	0.004
			0.15	0.092	347.4	12.2	89.9	0.08	0.0675	0.148	0.002
0.17[22]	61.5	410[24]	0.05	0.03	167.6	44.0	84.3	0.025	0.0233	0.049	0.001
			0.07	0.042	234.9	37.9	96.1	0.036	0.033	0.069	0.001
			0.12	0.073	405.1	26.3	129.3	0.063	0.0549	0.118	0.002
			0.15	0.092	509.3	21.4	149.6	0.078	0.0657	0.145	0.005
0.15[22]	54.3	350[24]	0.5	0.036	1683.3	0.98	724	0.297	0.191	0.488	0.012
			0.7	0.059	2764	0.173	1702	0.425	0.255	0.68	0.019

Table 3. Continued

Input				Output						
$Wt.\%FeO$	$\bar{c}_{Fe^{2+}}(mol \cdot m^{-3})$	$j_0(kA \cdot m^{-2})$	$V_{app}(V)$	$\eta_s(mV)$	$j(A \cdot m^{-2})$	$c^A_{Fe^{2+}}(mol \cdot m^{-3})$	$c^C_{Fe^{2+}}(mol \cdot m^{-3})$	$\eta_{AR}(V)$	$\eta_{RC}(V)$	$\eta_{AC}(V)$	$iR(V)$
			0.85	0.083	3912.5	0.055	3488	0.51	0.308	0.818	0.032
			1	1.13	5367.6	0.022	5930	0.578	0.347	0.925	0.075
			1.2	1.72	8104	0.013	13 736	0.617	0.409	1.026	0.174
			1.4	2.48	11 753	0.0115	27 078	0.62	0.459	1.089	0.311
			2	5.67	26 922.3	0.0113	193 197	0.627	0.605	1.23	0.77
			3	7.23	34 461.1	0.01	310 339	0.636	0.64	1.276	1.724

Table 3. A comprehensive summary of calculated results.

the bulk and at the surface of electrodes, activation/concentration overpotential, Ohmic potential drop, and current density. A transient calculation was performed but only final steady state results are subject to further analysis. A summary of all the calculated results (absolute values) is described in Table 3. It must be stated that currently the relationship among current density and applied voltage cannot be established due to a presence of several ad hoc parameters such as λ_s in the model.[17,18,20] Here, the applied voltage solely represents the driving force to impose a certain amount of electric current through the electrochemical system. Prange et al.[21] conducted an experiment on CaF_2–FeO slag to study the kinetics of the charge transfer reaction for the ferrous ion (Fe^{2+}) at 1723 K (1450° C) using the double pulse technique. Furthermore, Nowack et al.[22] analyzed the identical system to assess concentration overpotential at electrode surfaces. The results have been validated against their experiments.

As previously mentioned, a great advantage of the model is the direct calculation of field structures (e.g., electric potential field) across the electrolyte. Figure 2b and c indicates the electric potential and the ferrous concentration fields for various bulk concentrations of ferrous ion, also reported in Table 3, subjected to three different applied voltages (0.07, 0.12, and 0.15 V).Variation in the average bulk concentration of the ferrous ion strongly influences the system's behavior through the exchange current density. In other words, with the increase of bulk concentration of the ferrous ion at constant applied voltage, the system allows higher current density to flow through the slag. As shown in Figure 2c, with the increase of applied voltage, the distribution of the ferrous concentration alters in the vicinity of the anode/cathode. However, variation in ferrous concentration has no influence on the electric potential field as long as the applied voltage is kept constant as shown in Figure 2b. This implies that the electric potential field is dominantly determined by the distribution of non-reacting ions. The cation (Ca^{+2}) moves toward the cathode and anions (O^{2-} and F^{-}) accumulate near the anode. The thermal field near the electrodes is governed by Joule heating, while Joule heating is directly related to the potential drop. The stronger potential drop near the anode (electrode-positive) than that near the cathode (electrode-negative) may well explain the in-situ observation of higher melt rates for anodic electrodes than the cathodic one in the DC-operated ESR process.[15]

Below 1600 A m^{-2}, a linear relationship between current density and surface (activation) overpotential was reported by Prange et al.[21] As illustrated in **Figure 3**a, concentration overpotential due to a presence of ion concentration gradient between the bulk of slag and electrode–slag interface rises over time. As such, the activation overpotential is more precisely assessed in the experiment during a short time (e.g., here 0.6 μs). Furthermore, the concentration overpotential develops faster at higher current densities (e.g., here >1300 A m^{-2}). As shown in Figure 3a, strong agreement is observed between simulation and experimental results below 700 A m^{-2}, when the concentration overpotential remains negligibly small at

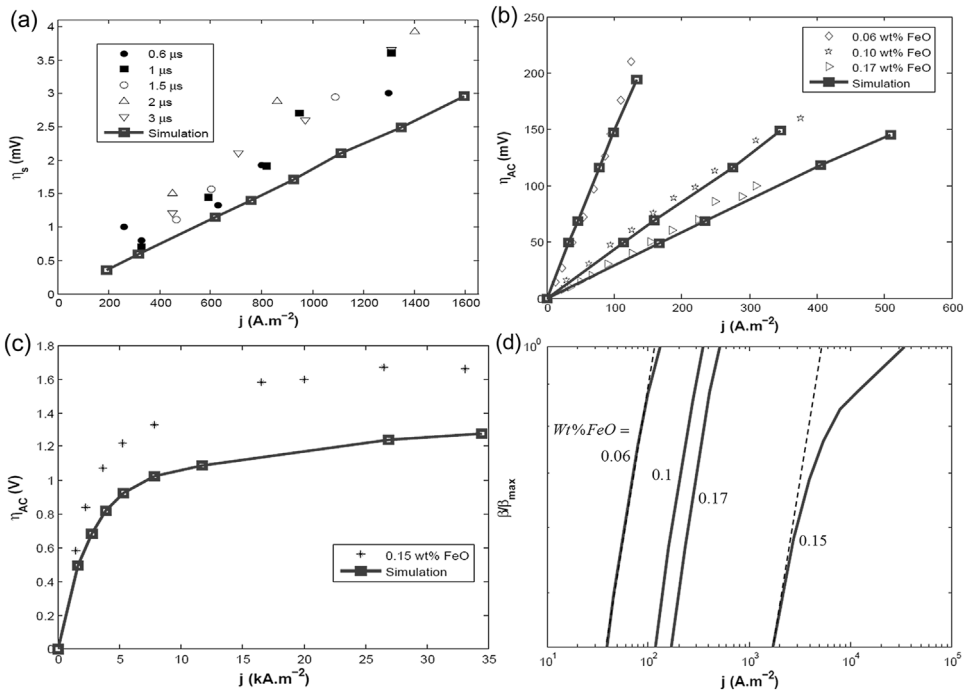

Figure 3. a) A comparison is made between simulation results and experimental data regarding to the activation (surface) overpotential which are reproduced from the experiment performed by Prange et al.[21]; in b) and c) the relationship among total concentration overpotential and current density obtained in the experiment conducted by Nowack[22] is compared with simulation results for b) low-current density, and c) large current density; d) The normalized β function (see **Table 1**) is plotted against the current density in logarithmic scale for different bulk concentration of FeO (0.06, 0.10, 0.15, and 0.17 wt% FeO).

short measuring times (0.6 μs). The accuracy of experimental data further decreases due to a strong development of concentration overpotential at high current densities. Accordingly, the discrepancy between simulation results and experimental data grows with the increase of current density (>700 A m^{-2}).

The relationship between the current density and concentration overpotential for various content of FeO is shown in Figure 3b. Apparently, the concentration overpotential is several orders of magnitudes larger than the activation (surface) overpotential even at lower imposed current density (< 500 A m^{-2}). The total concentration overpotential decreases strongly with increasing FeO content. There is strong agreement observed between the simulation results and the experiment. Consequently, the injection of ferrous ion at the anode and removal of ferrous ion at the cathode is a well-founded mechanism to explain the behavior of the system.[10] In contrast, a significant deviation is evident between experimental and simulation results at high current density (>2 kA m^{-2}), as shown in Figure 3c. Mitchell et al.[10] suggested that enrichment of ferrous ion (Fe^{2+}) at the anode and discharging calcium at the cathode takes place at a high current density. Then, the ferrous ion converts to the ferric (Fe^{3+}) iron and the calcium vaporizes, thus resulting in formation of gas bubbles in the slag.[10] Nowack et al.[22] asserted that altering the involved Faradaic reactions at slag–electrode interface significantly influences the relationship between concentration overpotential and current density. They suggested that variation in the slope of β function (Table 1), when the function is plotted against the current density on a logarithmic scale, can indicate the aforementioned modification of Faradaic reactions. Figure 3d shows β function plotted versus the current density in logarithmic scale for the simulation results. Obviously, a strong variation in the slope is obtained at high current density (>5 kA m^{-2}) although only one Faradaic reaction (Equations 8 and 9) is considered for all simulations. Furthermore, a comparison between the calculated and measured data shown in Figure 3c reveals that both experimental and simulation results follow the same trend, although a notable mismatch exists. It implies that altering Faradaic reactions may not be a correct approach to explain the relationship between current density and concentration overpotential for large imposed current in the CaF_2–FeO electrochemical system.

Aiming at applying the model for an industrial ESR process, further modeling steps are currently under development: the transport of other ions such as Al^{3+}, Si^{4+}, and Mg^{2+} within the conventional slag; the mechanism of ionic conduction involving electrochemical reactions at large current density (>40 kA m^{-2}), considering the flow and thermal fields.

4. Summary

We have addressed the necessity of developing an electrochemical model capable of describing the ion transport in the bulk of slag and electrochemical reactions at slag–metal interfaces for an ESR process. For that purpose, we propose a FVM-based numerical model to solve PNP equations, facilitating an evaluation of all relevant electrochemical parameters such as activation and concentration overpotential, as well as field structures like electric potential for the complex multi-ion electrochemical system. The model is tested on a one dimensional system: a DC electric current is applied to a molten multi-ion slag (CaF_2–FeO) between anode and cathode. Here, only the ferrous ion (Fe^{2+}) participates in the Faradaic reaction and all other ions (Ca^{2+}, F^-, and O^{2-}) are inert. We found that the maximum tolerable amount of current density at fixed voltage increases with the rise in the FeO concentration in the bulk, whereas the electric potential field remains unchanged. In other words, the potential field is governed by the distribution of non-reacting ions. The aforementioned findings may well explain the dependency of the melt rate on the electrode polarity for an ESR process as run under a DC current. With the increase of applied voltage, activation and surface overpotentials as well as Ohmic potential drop rise. From the relationship between the current density and concentration overpotential, we can deduce that iron oxidation at the anode and reduction of ferrous ion (Fe^{2+}) at the cathode, Equations 8 and 9, are the governing redox reactions at low current density below approximately $2\,kA\,m^{-2}$.[10] However, the previously proposed altering Faradaic reactions such as formation of ferric iron (Fe^{3+}) or a calcium discharge may not be a convincing explanation for the behavior of the CaF_2–FeO system at elevated current densities ($>5\,kA\,m^{-2}$). Although the model was tested against the available experiments,[21,22] we believe that further evaluation efforts are still required to make the model applicable for industry ESR process.

Acknowledgements

The authors acknowledge the financial support by the Austrian Federal Ministry of Economy, Family and Youth and the National Foundation for Research, Technology and Development within the framework of the Christian Doppler Laboratory for Advanced Process Simulation of Solidification and Melting.

Received: January 9, 2017; Revised: February 27, 2017; Published online: March 17, 2017

Keywords: activation overpotential; concentration overpotential; electric potential; electroslag remelting (ESR); faradaic reaction; ferrous ion; numerical modeling

References

[1] V. Weber, A. Jardy, B. Dussoubs, D. Ablitzer, S. Ryberon, V. Schmitt, S. Hans, H. Poisson, *Metall. Mater. Trans. B* **2009**, *40*, 271.
[2] A. Kharicha, M. Wu, A. Ludwig, E. Karimi-Sibaki, *Metall. Mater. Trans. B* **2016**, *47*, 1427.
[3] K. Fezi, J. Yanke, M. J. M. Krane, *Metall. Mater. Trans. B* **2015**, *46*, 766.
[4] N. Giesselmann, A. Rückert, M. Eickhoff, H. Pfeifer, J. Tewes, J. Klöwer, *ISIJ Int.* **2015**, *55*, 1408.
[5] E. Karimi-Sibaki, A. Kharicha, J. Bohacek, M. Wu, A. Ludwig, *Adv. Eng. Mater.* **2016**, *18*, 224.
[6] M. E. Fraser, A. Mitchell, *Ironmak. Steelmak.* **1976**, *5*, 279.
[7] Q. Wang, Z. He, G. Li, B. Li, C. Zhu, P. Chen, *Int. J. Heat Mass Trans.* **2017**, *104*, 943.
[8] M. E. Peover, *J. Inst. Met.* **1972**, *100*, 97.
[9] M. Barati, K. S. Coley, *Metall. Mater. Trans. B* **2006**, *37*, 51.
[10] A. Mitchell, G. Beynon, *Metall. Trans.* **1971**, *2*, 3333.
[11] M. Etienne, *PhD. Thesis*, UBC, Canada **1971**.
[12] Y. Kojima, M. Kato, T. Toyoda, M. Inouye, *Trans. ISIJ* **1975**, *15*, 394.
[13] E. Karimi-Sibaki, A. Kharicha, J. Bohacek, M. Wu, A. Ludwig, *Metall. Mater. Trans. B* **2015**, *46*, 2049.
[14] A. Kharicha, M. Wu, A. Ludwig, A. Ramprecht, H. Holzgruber, *CFD Modeling and Simulation in Materials Processing*, Wiley–Interscience, New Jersay, USA **2012**, p. 139.
[15] M. Kawakami, K. Nagata, M. Yamamura, N. Sakata, Y. Miyashita, K. S. Goto, *Testsu-to-Hagane* **1977**, *63*, 2162.
[16] J. Newman, K. E. Thomas-Alyea, *Electrochemical Systems*, John Wiley & Sons, New Jersay, USA **2004**.
[17] M. Z. Bazant, K. T. Chu, B. J. Bayly, *SIAM J. Appl. Math.* **2005**, *65*, 1463.
[18] K. T. Chu, M. Z. Bazant, *SIAM J. Appl. Math.* **2005**, *65*, 1485.
[19] E. Karimi-sibaki, A. Kharicha, M. Wu, A. Ludwig, *IOP Conf. Series Mater. Sci. Eng.* **2016**, 143, article 012008. doi:10.1088/1757899X/143/1/012008.
[20] E. Karimi-Sibaki, A. Kharicha, M. Wu, A. Ludwig, J. Bohacek, *J. App. Math. Comput.* **2016**, accepted.
[21] R. Prange, K. Heusler, K. Schwerdtfeger, *Metall. Trans. B* **1984**, *15*, 281.
[22] Nowack, K. Schwerdtfeger, D. Krause, *Arch. Eisenhüttenwes.* **1982**, *12*, 463.
[23] W. Chiho, X. Shunhua, *ISIJ Int.* **1993**, *33*, 239.
[24] J. Douglas Ray, *PhD. Thesis*, McMaster University, Canada **1981**.